Turbulent thermal convection in a finite domain: Part I. Theory

L. Sirovich and H. Park
Center for Fluid Mechanics and The Division of Applied Mathematics, Brown University, Providence, Rhode Island 02912

(Received 10 January 1990; accepted 8 May 1990)

Determination of the empirical eigenfunctions for turbulent flows, which result from the Karhunen–Loève procedure, is considered in some generality for fully inhomogeneous flows. Group theoretical considerations are shown to lead to considerable increases in an available database. In addition, group representation procedures are shown to lead to substantial simplification. In fact, for the application considered here, a nonmanageable problem is reduced to one that is solvable. The general methods and techniques presented here are applied to the case of Rayleigh–Bénard convection in a finite box. In addition, indication is made of how to apply the procedures to several other cases. Some results of applying the method of empirical eigenfunctions to a numerical simulation of this particular flow [H. Park and L. Sirovich, Phys. Fluids A 2, 1659 (1990)] are presented here.

I. INTRODUCTION

A central problem confronting turbulence research is the method by which to analyze and assess the vast databases being generated through experiment and computation. Traditional statistical averages of a flow and its moments remain of great value, but do not make full use of the data nor do they serve as a convenient method for storing data.

A method, complementary to the standard statistical theory, is based on the Karhunen–Loève (K–L) procedure,[1] a brief description of which is given in Sec. III. This is the method first suggested by Lumley[2-4] as a rational procedure for the extraction of coherent structures. Although it now seems unlikely that the method indeed accomplishes this goal,[5] the method is of unquestioned value in extracting essential features of the flow. As originally presented by Lumley and used by a number of investigators,[6-8] the method becomes impractical unless all but one of the directions are homogeneous. In the present paper we deal with a particular flow for which this *standard method* is inapplicable and consider instead a general procedure, the *method of snapshots*, for the analysis (see Sec. III). The particular case considered is that of the simulation of a confined, time stationary, fully inhomogeneous three-dimensional chaotic Rayleigh–Bénard flow (R–B)[9] hereafter referred to as (II).

The K–L procedure uses the two-point correlation function as an integral kernel for the generation of a complete set of eigenfunctions—which we refer to as the *empirical eigenfunctions*. For rectilinear geometries an unbounded direction is homogeneous and leads to sinusoidal dependence, in that direction, in the eigenfunctions. This, for example, is the case for the channel flow simulations[8,10,11] and in R–B simulations.[12-15] Each of the cited cases contain two homogeneous directions and as a result the empirical eigenfunctions are entirely factorable with the homogeneous directions being represented by sinusoids. Lumley,[2] recognizing that sinusoidal dependence is incompatible with the known compactness of a coherent structure, suggested a *shot noise* approximation for assembling these factorable eigenfunctions. Lumley's approach was given a thorough investigation by Moin and Moser,[8] in the framework of the channel problem. They show, by actual construction, that this results in *interesting flows*, which they refer to as characteristic eddies (but not coherent structures). (In Ref. 5 it is demonstrated, in generality, that the shot noise construction produces *flows* that carry smaller energies than the individual empirical eigenfunctions.)

For the case of a confined geometry the empirical eigenfunctions do not factor, and the shot noise hypothesis is not applicable. This case, therefore, furnishes a testbed for the notion that the empirical eigenfunctions yield (or are related to) the coherent structures of the flow. The evidence from our study is that this is not the case. The eigenfunctions that do emerge are complicated and interesting, but bear no obvious relationship to thermal plumes, which are the generally accepted coherent structures of R–B convection.

The confined R–B problem that is formulated and briefly discussed in Sec. II can be identified with the original treatment of the problem by Rayleigh.[16] Unlike other finite domain studies,[17,18] the case treated by us can be formulated as a pure initial value problem. The main physical discussion of the problem is reserved for (II), where the simulation is discussed and analyzed in some detail. The physical results that are discussed here, are included for the purpose of illustrating a methodology that is being applied to a fluid problem for the first time. Relatively extensive use of group theoretical methods appear in this paper. It is our belief that the approach taken has application to a general variety of fluid problems and the Appendix summarizes the method as applied to several other geometries.

While group theoretical ideas were implicitly in use, throughout the development of fluid mechanics, perhaps the first systematic use of group theory appeared in the book by Birkhoff.[19] This, and later books[20,21] stressed the consequences of similitude. More recently, Golubitsky *et al.*[22] and McKenzie[23] have shown the importance of group methods in studying bifurcation phenomena. The present investigation makes yet another use of group theory. We show that through the use of group representation theory we are able to treat an otherwise daunting calculation. Of equal impor-

 0899-8213/90/091649-10$02.00

tance is the fact that this approach systematically reduces the admissible flow structures to well-defined classes. For example, for the R–B problem studied here, just ten classes of *flows* appear. Each has its own symmetry and each has a physical interpretation.

To illustrate this point with a simple example, the symmetries of a problem often allow us to state that functional dependences are odd or even in a dependent variable. This of course simplifies a problem. The methods presented here permit us to exhaust all such simplifications. In the Appendix we sketch how methods can be applied to several other problems.

II. FORMULATION AND STABILITY CONSIDERATIONS

We consider a fluid confined to a rectangular parallelepiped as sketched in Fig. 1. The temperatures of the horizontal boundaries are held at $\mathscr{T} = T_0 + \Delta T/2$ and $\mathscr{T} = T_0 - \Delta T/2$ as indicated in the figure, while the side walls are taken to be insulating, $\partial\mathscr{T}/\partial n = 0$ (n a normal direction). In the absence of convection the temperature $\mathscr{T}$ and pressure P are given by their equilibrium values

$$\mathscr{T} = T_0 + (T_1 - T_0)z/H = T_0 - \beta z \tag{1}$$

and

$$P/\rho = -gz - \alpha\beta(z^2/2)g, \tag{2}$$

respectively. The notation is standard.[24,25]

The departure from equilibrium is governed by the Boussinesq equations

$$\begin{aligned} &\nabla\cdot\mathbf{u} = 0, \\ &\frac{\partial}{\partial t}\mathbf{u} + (\mathbf{u}\cdot\nabla)\mathbf{u} + \nabla p = \mathrm{Ra}\,\mathrm{Pr}\,\mathbf{e}_z T + \mathrm{Pr}\,\nabla^2\mathbf{u}, \\ &\frac{\partial T}{\partial t} + (\mathbf{u}\cdot\nabla)T = w + \nabla^2 T, \end{aligned} \tag{3}$$

where Pr and Ra represent the Prandtl and Rayleigh numbers:

$$\mathrm{Pr} = \nu/\kappa, \quad \mathrm{Ra} = g\alpha\beta H^4/(\kappa\nu). \tag{4}$$

In (3) T and p are departures from $\mathscr{T}$ and P as given by (1) and (2).

On taking the divergence of the momentum equation we can formally solve for the pressure, and eliminate it from (3). The system can then be written in the form

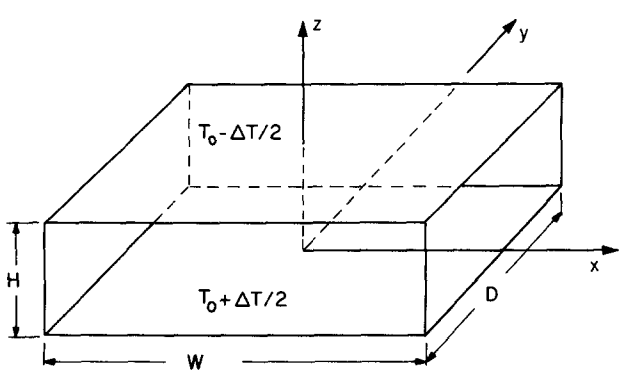

FIG. 1. Flow geometry. In the calculation itself the planform is a square, $W = D$.

$$\partial_t \begin{bmatrix} u_i \\ T \end{bmatrix} = \begin{bmatrix} \mathrm{Pr}\,\delta_{ij}\Delta - \mathrm{Ra}\,\mathrm{Pr}\,\Delta^{-1}\partial_i \\ \delta_{3j} \quad \Delta \end{bmatrix} \begin{bmatrix} u_j \\ T \end{bmatrix} - \begin{bmatrix} (\delta_{ik}\partial_l + \Delta^{-1}\partial^3_{ikl})u_k u_l \\ \partial_k(u_k T) \end{bmatrix}, \tag{5}$$

where Δ refers to the Laplace operator and Δ^{-1} its formal inverse. It should be noted that the incompressibility condition $\nabla\cdot\mathbf{u} = 0$, now becomes an initial condition for the system (5).

If we denote the *state* of the fluid by $\mathbf{V} = (\mathbf{u}, T)$, and the linear part of the right-hand side of (5) by L, then

$$\partial_t \mathbf{V} = \mathbf{L}\mathbf{V} + \mathbf{N}(\mathbf{V}) \tag{6}$$

with the $\mathbf{N}(\mathbf{V})$ the nonlinear remainder term. The boundary conditions on the temperature are given by

$$\begin{aligned} 0 = T(0) = T(H) = \frac{\partial T}{\partial x}(0) \\ = \frac{\partial T}{\partial x}(W) = \frac{\partial T}{\partial y}(0) = \frac{\partial T}{\partial y}(D). \end{aligned} \tag{7}$$

Thus the temperature is fixed on the upper and lower walls while the side walls are insulating. Although lengths have been scaled by H, so that W and D really refer to W/H and D/H, it is convenient in (7) and elsewhere to retain the original symbols and think of them as being dimensionless. To further fix the problem we consider the case of *slippery* boundary conditions,

$$\mathbf{u}\cdot\mathbf{n} = 0 = \frac{\partial}{\partial n}(\mathbf{n}\wedge\mathbf{u}) \tag{8}$$

at each bounding plane, where $\mathbf{n}$ denotes the normal.

The stability of the equilibrium solution is determined by the eigentheory of the linear operator, $\mathbf{L}$, viz.,

$$\mathbf{L}\phi = \lambda\phi, \tag{9}$$

where ϕ is a four-component vector function of position $\mathbf{x}$. Under the boundary conditions (7) and (10), the eigenfunctions have the form

$$\phi = \begin{bmatrix} u_0 \sin(k_1 x)\cos(k_2 y)\cos(k_3 z) \\ v_0 \cos(k_1 x)\sin(k_2 y)\cos(k_3 z) \\ w_0 \cos(k_1 x)\cos(k_2 y)\sin(k_3 z) \\ \tau_0 \cos(k_1 x)\cos(k_2 y)\sin(k_3 z) \end{bmatrix}, \tag{10}$$

where

$$k_1 = \frac{n_1\pi}{W}, \quad k_2 = \frac{n_2\pi}{D}, \quad k_3 = \frac{n_3\pi}{H}, \tag{11}$$

n_1, n_2, n_3 are integers, and u_0, v_0, w_0, τ_0 constants. The only eigenvalue of (9) which can change signature is given by

$$\lambda = \frac{-k^2(1+\mathrm{Pr})}{2} + \sqrt{\frac{(1-\mathrm{Pr})^2 k^4}{4} + \frac{k_1^3 \mathrm{Ra}}{k^2}}, \tag{12}$$

where

$$k_1^2 = k_1^2 + k_2^2. \tag{13}$$

The corresponding eigenvector is

$$\mathbf{v}_0 = [k_1 k_3, k_2 k_3, -k_1^2, -(\lambda + \mathrm{Pr}\,k^2)k^2/\mathrm{Ra}\,\mathrm{Pr}], \tag{14}$$

which is seen to be incompressible.

When $\lambda = 0$ we obtain the critical Rayleigh number Ra_0, given by

$$\mathrm{Ra}_0 = \frac{k^6}{k_\perp^2} = \frac{\pi^4(H^2 n_1^2/W^2 + H^2 n_2^2/D^2 + n_3^2)^3}{(n_1^2/W^2 + n_2^2/D^2)}. \tag{15}$$

The minimum value, Ra_c, of (15), is

$$\mathrm{Ra}_c = 27\pi^4/4 \tag{16}$$

and is achieved when

$$n_3^2 = 1 \tag{17}$$

and

$$n_1^2 H^2/W^2 + n_2^2 H^2/D^2 = \tfrac{1}{2}. \tag{18}$$

The minimum critical Rayleigh number, Ra_c, is the classical value found for two-dimensional rolls in a horizontally infinite domain.[24] To make contact with the unbounded case note that if $D \uparrow \infty$ then the smallest most unstable *width* is $W/H = \sqrt{2}$ in contrast with the classical value of $2\sqrt{2}$. But for the case being discussed here only one roll occurs while in the standard situation two counter-rotating rolls occur (a full wave). Thus the two situations agree.

At first sight it might seem contradictory for us to obtain the same minimum critical Rayleigh number as in the horizontally unbounded case, since the case under investigation would appear to be more restrictive (geometrically) and thus should become unstable at a higher Ra number. To reconcile the apparent contradiction it should be noted that the problem under investigation is solvable as an initial value problem that can be posed in the infinite domain. As a result it also leads to the minimal Rayleigh number, (16), as do a number of other finite geometries. The present geometry was in fact considered by Rayleigh in his original stability analysis.[16] Extensions have been given by Pellew and Southwell[17] and Davis.[18]

For reasons to be discussed in the next section the case of a square cross section will be considered, i.e., $W = D$. Thus the smallest cell supporting the most unstable mode is one for which

$$W = D = 2H. \tag{19}$$

Figure 2 shows some representative streamlines of the most unstable mode using (14) in (10). The vertical midplane is a symmetry plane of the motion. Also the motion is invariant under rotations of a quarter turn around the vertical centerline. This vertical axis is also a locus of stagnation points for the flow.

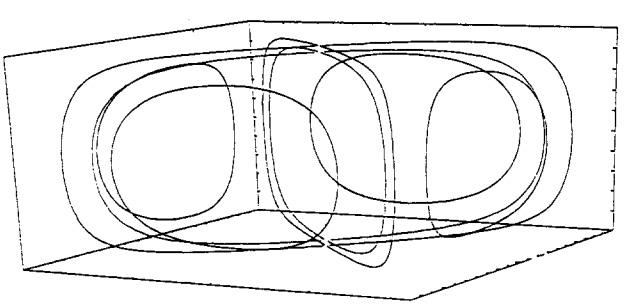

FIG. 2. The most unstable mode from linear stability. This mode remains unchanged under rotations of $\pi/2$, with the vertical centerline a stagnation point locus.

III. KARHUNEN–LOÈVE EIGENFUNCTIONS

In (II) we report on the results obtained by numerically integrating the Boussinesq equations for the nonlinear problem formulated in Sec. II, at a Rayleigh number for which the flow is weakly turbulent or *chaotic* ($\mathrm{Ra} = 70\mathrm{Ra}_c$). The flow, which is statistically stationary, is then analyzed by means of the (K–L) expansion. This technique has been adopted by a number of investigators and is an important tool for the analysis of turbulent flows. For completeness we briefly outline the method and follow a somewhat different approach, one that is especially suited to the turbulent flow being considered here.[26]

A turbulent flow can be characterized as a point, moving in a representational space, which in the present instance is infinite dimensional. The location of this point, or *state*, fully describes the flow at each instant of time. After an initial transient the point is drawn into the attracting set for the system and moves in a chaotic fashion on this set, termed the *chaotic attractor*. The current evidence is that for closed dissipative systems, such as (3), the dimension of this attractor is low.[27–30] The flow is time stationary, and under the ergodic assumption, ensemble averages of flow quantities (denoted below by brackets) can be regarded as time averages on the attractor. It is shown in the next section, that group theoretical consideration considerably extend our time records.

For the case of a horizontally unbounded flow the mean velocity, $\langle \mathbf{u} \rangle$, vanishes. This is a direct consequence of horizontal homogeneity. Homogeneity is lost for the bounded case and $\langle \mathbf{u} \rangle \neq 0$. Figure 3, with some fine print discussed in Sec. V, depicts the mean velocity. We see that it is composed of two cells, which are mirror images of one another, in the horizontal centerplane. The maximum value of the velocity is small and in the present normalization this is

$$\max_{\mathbf{x}} |\langle \mathbf{u} \rangle| = 0.115. \tag{20}$$

The mean temperature $\langle T \rangle$ is in general a function of (x,y,z) although the dependence on the first two variables proves to be weak. This is illustrated in Fig. 4, which shows the actual temperature profiles from (II) at a number of locations in the cell. As can be seen there is a buildup of heat flow, due to convection, in the four corners of the cell. Thus the corners accommodate the transport of heat across the chamber.

For later purposes it is useful to define the horizontally averaged temperature,

$$\overline{T} = \frac{1}{WD} \int_0^W \int_0^D \langle T \rangle dx\, dy = \overline{T}(z) \tag{21}$$

and then write

$$T = \overline{T} + \theta. \tag{22}$$

Then instead of $\mathbf{V}$, we consider as a state variable

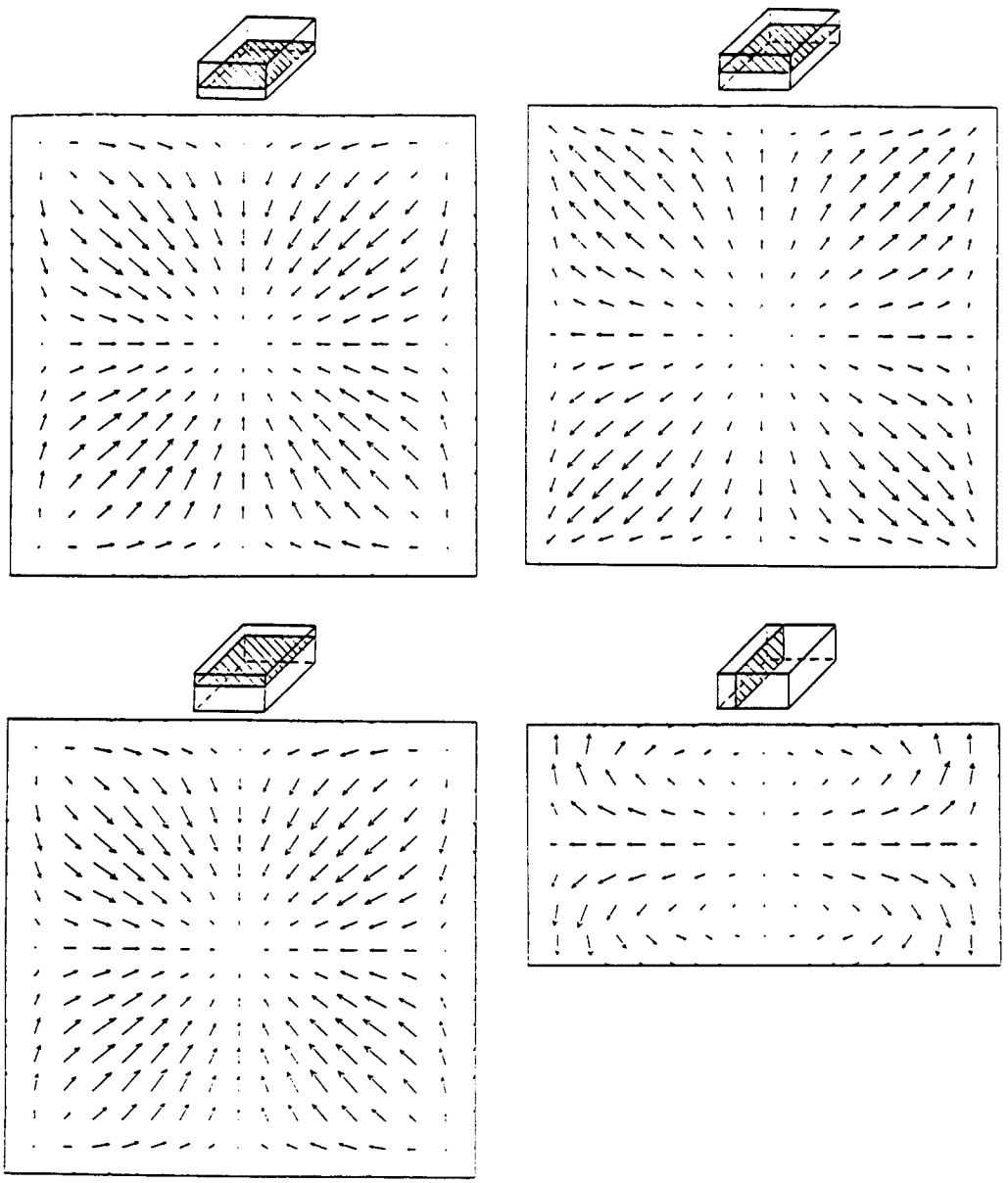

FIG. 3. Ensemble-averaged mean flow.

$$\mathbf{v} = (\mathbf{u},\theta) \tag{23}$$

the flow *fluctuation*. (In view of the smallness of $|\langle \mathbf{u} \rangle|$ we do not remove the mean velocity.)

It is clear that there is some arbitrariness and trade-offs in the choice of the fluctuation $\mathbf{v}$. As a general rule one wants to subtract off the mean and only deal with departures from the mean. In this way we do not have to repeatedly consider what is implicitly contained in each member of the set, viz., the mean. For computational purposes it is useful to deal with a horizontal average $\overline{T}$, instead of $\langle T \rangle$. Carrying such small differences is tolerable and we also do this for $\langle \mathbf{u} \rangle$.

Imagine an ensemble of states or *snapshots* of the flow on the attractor,

$$\mathbf{v}^{(n)} = \mathbf{v}(\mathbf{x},t_n), \tag{24}$$

sampled at uniformly spaced, uncorrelated times t_n. To arrive at the K–L procedure one can seek the *most likely state*, say given by $\phi(x)$, in the sense that

$$\lambda = \langle (\mathbf{v}^{(n)},\phi)^2 \rangle \tag{25}$$

is a maximum, subject to the normalization condition

$$(\phi,\phi) = \int \sum_k \phi_k(\mathbf{x})\phi_k(\mathbf{x})d\mathbf{x} = 1. \tag{26}$$

The solution to this problem is given by the principal eigenfunction of

$$\mathbf{K}\phi = \int \mathbf{K}(\mathbf{x},\mathbf{x}')\phi(\mathbf{x}')d\mathbf{x}' = \lambda\phi(\mathbf{x}), \tag{27}$$

where

$$K_{ij}(\mathbf{x},\mathbf{x}') = \langle v_i(\mathbf{x})v_j(\mathbf{x}') \rangle = \frac{1}{M}\sum_{n=1}^{M} v_i^{(n)}(\mathbf{x})v_j^{(n)}(\mathbf{x}') \tag{28}$$

is the two-point correlation function and M is the number of snapshots that have been collected. (When not confusing the superscript n will be dropped as in the brackets above.)

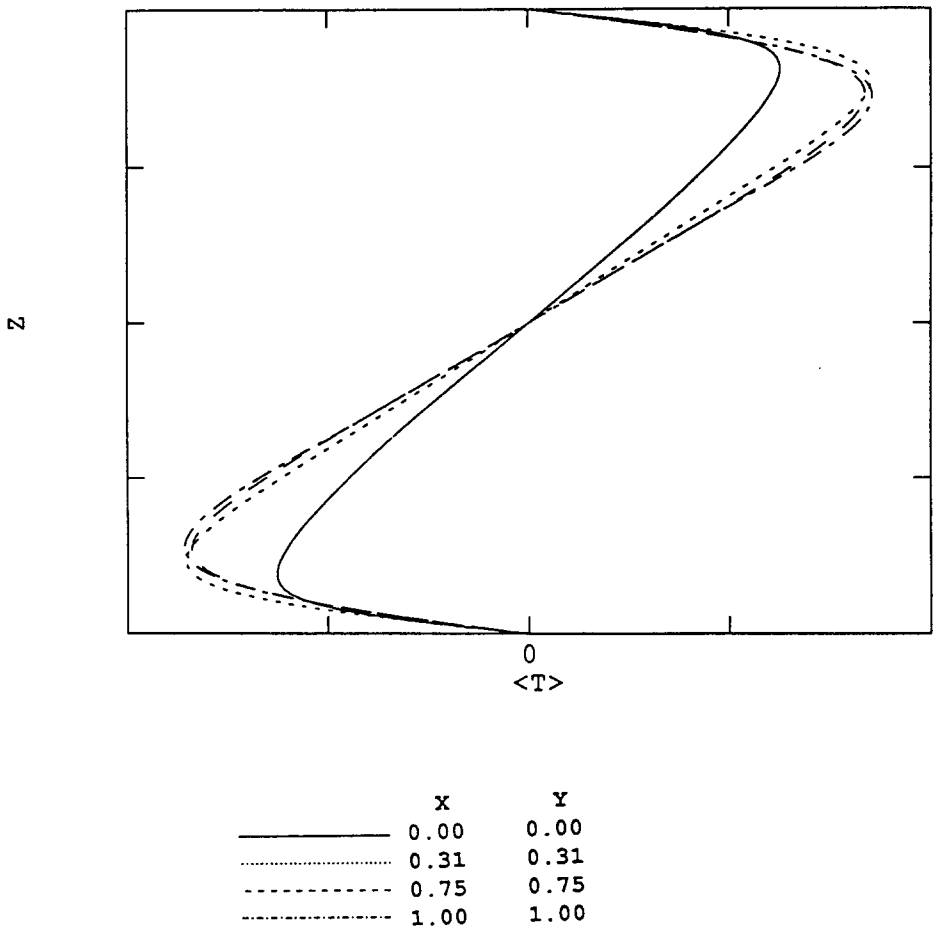

FIG. 4. Temperature variation at several (x,y) locations.

Here, **K** is a non-negative Hermitian operator and relation (27) generates a complete orthornormal set $\{\phi_n\}$ with $\lambda_n \geqslant 0$.

Finally except for a set of zero measure the flows can be expanded in the eigenfunctions $\{\phi_n\}$

$$\mathbf{v}(\mathbf{x},t) = \sum_{n=1} a_n(t)\phi_n(x), \tag{29}$$

where convergence is in the L_2 sense. The coefficients a_n are uncorrelated in time, i.e., they are statistically orthogonal

$$\langle a_n a_m \rangle = \lambda_n \delta_{nm}. \tag{30}$$

This is the essential content of the K–L procedure.[1] These and related properties of the procedure strongly recommend the use of the resulting empirical eigenfunctions in problems of turbulent flows.

To assess the computation necessary to carry out the K–L procedure consider the R–B convection problem formulated in Sec. II. For a pseudospectral method with N points on a side, N^3 grid points are involved. There are also three dependent variables [the three velocities are related through continuity (3)]. Thus a matrix approximation to **K** will have $(3\times N^3)^2$ entries. Even for the most modest grid, such an undertaking would exceed present computer resources. For a one-dimensional calculation (Sirovich and Rodriguez, 1987) the method proves feasible.[31] Also, in problems with two homogeneous directions such as the R–B problem without side walls[13–15] and plane Poiseuille flow without side walls,[8] the eigenfunction dependence on the homogeneous directions are accounted for by sinusoids and the eigenfunction problem, (27), is reduced to an equivalent one-dimensional problem.

For the case being treated here, no homogeneous directions exist. One can however resort to the *method of snapshots*. This is based on the fact that (30) is a degenerate kernel[32] and therefore that an eigenfunction of **K** has the representation

$$\phi(\mathbf{x}) = \sum_{n=1}^{M} \alpha_n \mathbf{v}^{(n)}(x), \tag{31}$$

i.e., an eigenfunction is an admixture of snapshots. The problem of determining the coefficients α_n is thus reduced to dealing with an $M \times M$ matrix. To see this, we substitute (31) into (27), where **K** is given by (28). Therefore if we define

$$C_{mn} = (\mathbf{v}^{(m)},\mathbf{v}^{(n)})/M \tag{32}$$

and the set $\alpha = (\alpha_1,\alpha_2,...,\alpha_M)$, then

$$\mathbf{C}\alpha = \lambda\alpha \tag{33}$$

is the matrix problem that determines the eigenvalues and eigenfunctions. It is clear that this determines just M of the empirical eigenfunctions. The remaining infinitude of eigenfunctions are not uniquely determined. The only requirement on them is that they be orthogonal to the already deter-

mined set and hence orthogonal to $\{\mathbf{v}^{(n)}\}$. They belong to the null space of $\mathbf{K}$. An immediate consequence of (31) is that each eigenfunction is an incompressible flow. (This procedure has been successfully used in an entirely different application.[33,34])

IV. SYMMETRY CONSIDERATIONS

The numerical simulation of R–B convection reported on in (II) is for the case of a square cross section, $W = D$, see Fig. 1. This case generates a maximal amount of symmetry and as we will see this furnishes us with a number of advantages both in the extension of the database and the treatment of the solutions.[35]

There are 16 elements in the invariance group for the convective cell specified by

$$\frac{-W}{2} \leqslant x, \quad y \leqslant \frac{W}{2}, \quad \frac{-H}{2} \leqslant z \leqslant \frac{H}{2}.$$

(For purposes of exposition we temporarily transform to a coordinate system having its origin at the center of the cell.) In the (x,y) plane there are eight symmetries of the square, known as the dihedral group D_4 (Ref. 36). In addition to the identity I, there is for example the 90° rotation, R,

$$R(x,y,z,u,v,w,\theta) = R(\mathbf{x},\mathbf{v}) \to (-y,x,z,-v,u,w,\theta). \tag{34}$$

The new flow generated by (34), satisfies the Boussinesq equations, (3), as well as the boundary conditions, (7) and (8). It therefore generates an admissible solution to the posed problem. Other new flows are generated by each of the group elements that we now define.

It is clear that (34) implies that admissible flows are also generated by the 180° rotation R^2 and by the 270° rotation R^3. Other admissible solutions to the flow problem are generated as follows: Reflection along the x axis, denoted by X,

$$X(\mathbf{x},\mathbf{v}) \to (-x,y,z,-u,v,w,\theta), \tag{35}$$

and similarly reflection along the y axis, denoted by Y. Next there is reflection in the line $y = x$, denoted by L,

$$L(\mathbf{x},\mathbf{v}) = (y,x,z,v,u,w,\theta) \tag{36}$$

and reflection in $y = -x$ denoted by D. In all the eight elements of D_4 are

$$D_4: I, R, R^2, R^3, X, Y, L, D. \tag{37}$$

In addition, and perhaps less intuitive, a new admissible solution is produced by reflection along the z axis,

$$Z(\mathbf{x},\mathbf{v}) \to (x,y,-z,u,v,-w,-\theta). \tag{38}$$

If the full group is denoted by G then the 16 elements of G are given by

$$G = D_4, ZD_4. \tag{39}$$

Also we will write $G = \{g_l\}$ with g_l, $l = 1,2,...,16$, denoting the group elements. The group table for D_4 is standard and for convenience and later reference is shown in Table I. Since Z commutes with D_4 and $Z^2 = I$ the group table for G is a simple extension of Table I.

We underline the fact that under each of the group operations, a new *admissible* flow is generated. If $\mathbf{v}$ satisfies the Boussinesq equations, (3), as well as the boundary conditions, (7) and (8), of the problem, then so does $g\mathbf{v}$ for each member, g, of G. Thus if $\{\mathbf{v}^{(n)}\}$ represents an ensemble of states generated by the numerical calculation in (II) then

$$\{g_l \mathbf{v}^{(n)}\}, \quad l = 1,...,16, \tag{40}$$

represents a 16-fold increase in the ensemble size and therefore in the database! The correlation kernel defined by (30) can now be reaveraged to give

$$\mathbf{K} = \frac{1}{J}\sum_{l=1}^{J} \langle g_l \mathbf{v}(\mathbf{x}) \mathbf{v}^{\dagger}(\mathbf{x}') g_l^{\dagger} \rangle = \frac{1}{J}\sum_{l=1}^{J} g_l \mathbf{k}(\mathbf{x},\mathbf{x}') g_l^{-1}. \tag{41}$$

Here,

$$\mathbf{k} = \langle \mathbf{v}(\mathbf{x}) \mathbf{v}(\mathbf{x}) \rangle = \langle \mathbf{v}^{(n)}(\mathbf{x}) \mathbf{v}^{(n)\dagger}(\mathbf{x}) \rangle \tag{42}$$

denotes the correlation tensor, not extended by the symmetries, and J is the number of group elements, which in the present instance is 16. Since each group element is easily seen to be a unitary transformation, the adjoint can be replaced by the inverses as we have in (41). It should be noted that as a result of the group average in (41), all time records (and hence all time averages) can be regarded as having been extended by a factor of 16.

In (II) we consider a numerical simulation for which $\{\mathbf{v}^{(n)}\}$ contains 200 *snapshots*. Thus under the group G we have the equivalent of 3200 ensemble members! While such an extension of the database is desirable it appears to be too much of a good thing since the direct use of 3200 *snapshots* to solve the eigenvalue problem, (29), would entail diagonalizing a 3200×3200 matrix which is somewhat excessive for present-day machines. However, a second application of group theory removes this difficulty, and as will be seen in the next section it is never necessary to deal with a matrix of order greater than 400×400, at one time.

TABLE I. The group table for D_4.

	I	R	R^2	R^3	X	L	Y	D
I	I	R	R^2	R^3	X	L	Y	D
R	R	R^2	R^3	I	D	X	L	Y
R^2	R^2	R^3	I	R	Y	D	X	L
R^3	R^3	I	R	R^2	L	Y	D	X
X	X	L	Y	D	I	R	R^2	R^3
L	L	Y	D	X	R^3	I	R	R^2
Y	Y	D	X	L	R^2	R^3	I	R
D	D	X	L	Y	R	R^2	R^3	I

V. REDUCTION BY GROUP REPRESENTATIONS

To motivate and illustrate this reduction, we point out that as a result of the reflectional symmetry in the vertical direction, it follows that the entries of an eigenvector, $\phi(\mathbf{x})$, are separately odd or even functions of z [the first two components of $\phi(\mathbf{x})$ are of one parity and the last two of opposite parity in z]. Clearly parity considerations should split the calculation into two separate parts. Other such splittings of the calculation are apparent and in the following we show how to systematically pursue such operations and thus en-

sure that all possibilities are being fully exploited. The result of this will not only simplify the calculations, but also will *dissect* a flow into its natural classes of motions.

For purposes of exposition we start by considering the action of Z, the vertical reflection, (38), on the original ensemble. Thus in the notation of (41) and (42) the extension of $\mathbf{k}$ by Z yields

$$\kappa = \tfrac{1}{2}\langle \mathbf{v}\mathbf{v}^\dagger \rangle + \tfrac{1}{2}\langle (Z\mathbf{v})(Z\mathbf{v}^\dagger)\rangle = \tfrac{1}{2}(\mathbf{k} + Z\,\mathbf{k}Z) \tag{43}$$

(since $Z^{-1} = Z$). The number of snapshots has been doubled by this action. Next consider the decomposition of unity,

$$I = (I - Z)/2 + (I + Z)/2 \equiv Z^- + Z^+. \tag{44}$$

From this it follows that

$$(Z^\pm)^2 = Z^\pm, \tag{45}$$

and

$$Z^+ Z^- = 0, \tag{46}$$

so that Z^+ and Z^- are orthogonal projectors. Next observe that

$$Z\kappa = \tfrac{1}{2}(Z\,\mathbf{k}Z^2 + Z^2\mathbf{k}Z) = \tfrac{1}{2}(Z\,\mathbf{k}Z + \mathbf{k})Z = \kappa Z. \tag{47}$$

(More generally the same argument shows that $g_l K = K g_l$.) It also follows that $Z^\pm$ both commute with κ and that

$$Z^\mp \cdot Z = Z \cdot Z^\mp = \mp Z^\mp. \tag{48}$$

Finally if we multiply κ by

$$I = I^2 = (Z^+)^2 + (Z^-)^2 \tag{49}$$

we obtain

$$\kappa = \kappa^+ + \kappa^-, \tag{50}$$

where

$$\kappa^\pm = \langle (Z^\pm \mathbf{v}^{(n)})(Z^\pm \mathbf{v}^{(n)})^\dagger \rangle. \tag{51}$$

Now suppose ϕ is an eigenfunction of κ,

$$\kappa\phi = \lambda\phi, \tag{52}$$

then it follows easily that

$$\kappa^\pm \phi = \lambda\phi. \tag{53}$$

The kernels κ^+ and κ^- are clearly orthogonal and an eigenfunction (of nonzero eigenvalue) of one belongs to the null space of the other.

From this it follows that we can separately consider the eigenfunctions of κ^+ and κ^-. As a result of the above discussion these are the eigenfunctions of κ itself. But from (51) each resulting calculation only involves an ensemble size equal to the original ensemble. (The new ensemble members, however, must be *conditioned* to be $\{Z^\pm \mathbf{v}^{(n)}\}$—which turns the vector entries into odd or even functions of Z.)

Consideration of the reflections X and Y would also lead to the same line of discussion. To obtain a systematic approach, leading to the full reduction, one can appeal to the theory of group representations (Burrow[37]). As it turns out, the two essential ingredients in the above procedure were finding the projectors $Z^\pm$ and the fact that these commute with the group elements. We now indicate how to do this in the plane (D_4). The basic features associated with the decomposition in the z direction have already been derived.

The *class operators* of a group by definition commute with the elements of the group. For D_4 the class operators are given by

$$I, \quad Q = R^2, \quad A = R + R^3, \quad B = X + Y, \quad C = L + D, \tag{54}$$

as may be verified by checking the group table (Table I). It is therefore reasonable to proceed by assuming that a desired projector $E (E^2 = E)$ is a linear combination of the class operators

$$E = \alpha I + \beta Q + aA + bB + cC, \tag{55}$$

where the constants are determined by the condition that E is a projector. The result of this calculation is the following list of projectors:

$$\begin{aligned} E_1 &= (I - Q)/2, \\ E_2 &= (I + Q + B - A - C)/8, \\ E_3 &= (I + Q + A - B - C)/8, \\ E_4 &= (I + Q + C - A - B)/8, \\ E_5 &= (I + Q + A + B + C)/8. \end{aligned} \tag{56}$$

That these are orthogonal projectors may be verified directly, and from inspection it follows that

$$I = \sum_{p=1}^{5} E_p = \sum_{p=1}^{5} E_p^2. \tag{57}$$

From this and the commutation property we may write

$$\mathbf{K} = \sum_{p=1}^{5} E_p \mathbf{K} E_p = \sum_{p=1}^{5} \mathbf{K}_p. \tag{58}$$

By virtue of the orthogonality of the projectors $\mathbf{E}_p$ it follows that the eigenfunctions, of the $\mathbf{K}_p$'s, corresponding to nonzero eigenvalues, are orthogonal for different subscripts p. Thus if

$$\mathbf{K}_p \phi = \lambda\phi, \quad \lambda \neq 0, \tag{59}$$

then

$$\mathbf{K}\phi = \lambda\phi. \tag{60}$$

A straightforward use of the group table shows that

$$\mathbf{K}_p = 8\langle (E_p \mathbf{v}^{(n)})(E_p \mathbf{v}^{(n)})^\dagger \rangle, \quad p \neq 1. \tag{61}$$

On going over to the full group G with K given by (41) we can write

$$\mathbf{K} = \sum_{p=1} (\mathbf{K}_p^+ + \mathbf{K}_p^-), \tag{62}$$

with

$$\mathbf{K}_p^\pm = 8\langle (E_p Z^\pm \mathbf{v}^n)(E_p Z^\pm \mathbf{v}^{(n)})^\dagger \rangle, \quad p \neq 1. \tag{63}$$

(The case of $p = 1$ requires special attention.) Thus each of the kernels $K_p^\pm$, $p = 2,3,4,5$ only involves an ensemble size equal to the original ensemble.

To treat the remaining case of $p = 1$ corresponding to E_1, (56), observe that after some manipulation

$$\begin{aligned} \mathbf{K}_1(w) = 2\{&\langle \mathbf{w}\mathbf{w}^\dagger \rangle + \langle (R\mathbf{w})(R\mathbf{w})^\dagger \rangle + \langle (X\mathbf{w})(X\mathbf{w})^\dagger \rangle \\ &+ \langle (XR\mathbf{w})(XR\mathbf{w})^\dagger \rangle\}, \end{aligned} \tag{64}$$

where

$$\mathbf{w} = E_1 \mathbf{v} = [(I - R^2)/2]\mathbf{v}. \tag{65}$$

It is useful to observe that the elements are odd in the origin of the (x,y) plane and hence

$$R^2\mathbf{w} = -\mathbf{w}. \tag{66}$$

In the context of the 200 base snapshots that we have been speaking about, the kernel $\mathbf{K}_1$ involves 800 renditions. This however can be further reduced. First we observe that $\mathbf{K}_1$ is invariant under the subgroup of *quarter turns*, R^n, $n = 0,1,2,3$. Thus if $\mathbf{V}$ represents an eigenfunction of $\mathbf{K}_1$ then $R^n\mathbf{V}$, $n = 0,1,2,3$ are also eigenfunctions:

$$K_1 R^n \mathbf{V} = \lambda R^n \mathbf{V}, \quad n = 0,1,2,3. \tag{67}$$

However in view of (67) $R^2\mathbf{V}$ and $R^3\mathbf{V}$ are just negatives of $\mathbf{V}$ and $R\,\mathbf{V}$.

This motivates the introduction of the *complex snapshot*

$$\omega = \mathbf{w} + iR\mathbf{w} \tag{68}$$

and the Hermitian kernel

$$\begin{aligned}\mathbf{K}_1(\omega) &= \mathbf{K}_1(\mathbf{w}) + [iRK_1(\mathbf{w}) - iK_1(w)R^{-1}]/2 \\ &= \langle \omega\omega^\dagger \rangle + \langle (X\omega)(X\omega)^\dagger \rangle. \end{aligned} \tag{69}$$

In terms of the eigenfunctions $\mathbf{V}$ and $R\,\mathbf{V}$ of K_1 the eigenfunctions of K_1 are

$$\Omega = \mathbf{V} + iR\,\mathbf{V}, \tag{70}$$

$$\mathbf{K}_1 \Omega = \lambda \Omega. \tag{71}$$

But the *snapshots* contained in $\mathbf{K}_1$ are $\{\omega^{(n)}\}$ and $\{X\omega^{(n)}\}$, and hence for the nominal case being discussed, just 400 in number. As outlined earlier in (62) we actually consider

$$K_1^{\pm} = K(Z \pm \omega). \tag{72}$$

This then completes the discussion of symmetries. As signaled earlier this has resulted in a 16-fold increase in the data with little additional computation.

We close this section by pointing out that the steps in arriving at both the extension of data sets and the subsequent reduction of the integral equations follow from straightforward procedures. These two procedures rest on determining the underlying invariance group of flow. Thus flows involving boundaries that are rectangular, circular, ellipses, regular polygons, and so forth are immediate candidates for the methodology of this paper. We give several illustrations of this in the Appendix.

VI. ADDITIONAL COMMENTS

Before commenting on the nature of the eigenfunctions, we point out that the problem of convection in an imperme-

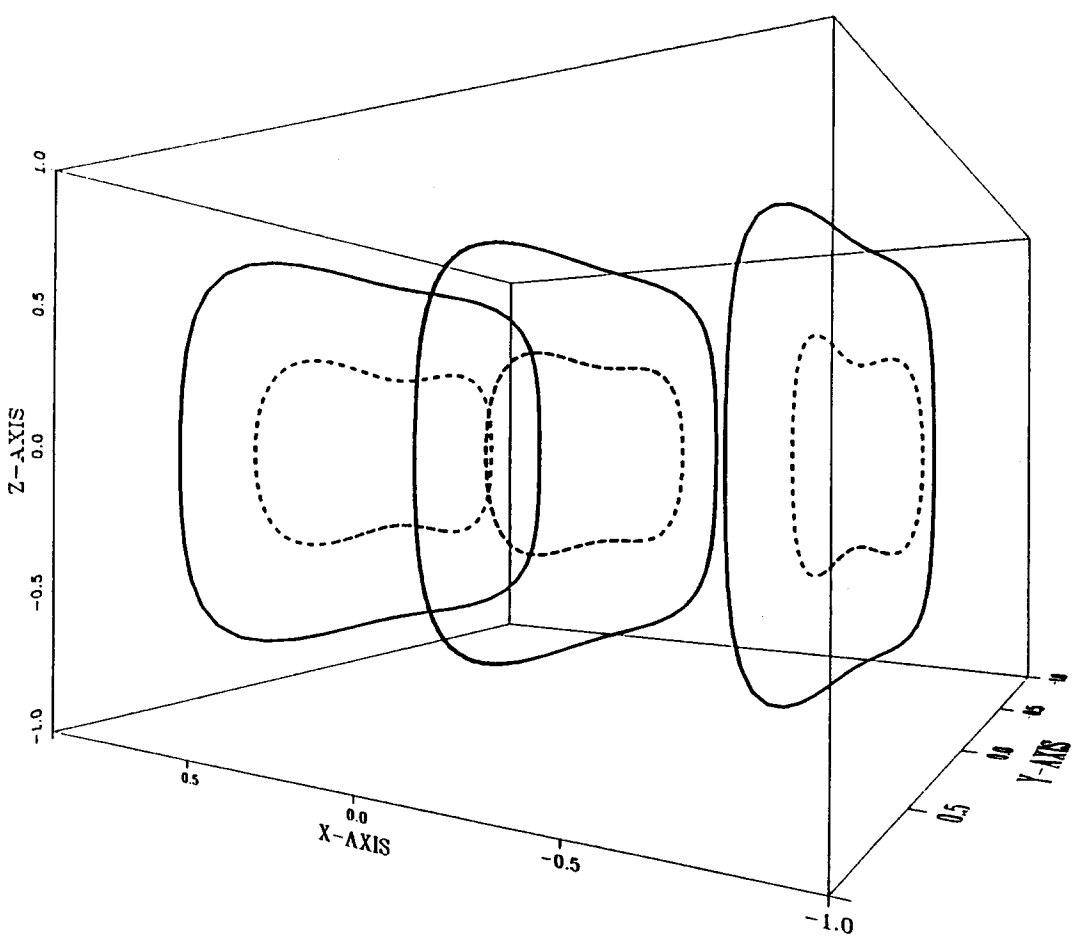

FIG. 5. Principal K–L eigenfunction. The motion is that of a roll along the y axis. The second member of the invariant subspace is obtained by rotation by $\pi/2$ about the vertical axis.

able cell with *slippery* boundary conditions that we have discussed is also related to the Taylor–Green problem.[38–40] In fact without the thermal forcing term the motion is of the same type as appears in the Taylor–Green problem. This motion as is well known ultimately decays to zero. The temperature difference between the upper and lower plates creates a buoyancy effect that drives the fluid, and by contrast with the Taylor–Green problem, the resulting flow reaches a statistically steady state.

It is of interest to contrast the K–L eigenfunctions with those that are obtained from the linear stability analysis presented in Sec. II. As is clear from (10) the eigenfunctions that result from stability analysis are in factorable form. The K–L eigenfunctions, as we have underlined several times, have their (x,y,z) dependence intertwined. Figure 5 indicates the streamline pattern for the principal eigenfunction, as calculated from the database in (II). This is seen to be mainly a rolling motion aligned along the y axis. It is important to realize however that the motion is not two dimensional. The closed loops shown in Fig. 5 do not lie in a plane.

Each of the eigenfunctions can be associated with one of the operators $\mathbf{K}_p^{\pm}$, $p = 1,2,...,5$. Thus the eigenfunctions of the full covariance operator $\mathbf{K}$ are naturally split into ten classes. It further follows from our discussion of $K_1^{\pm}$ in the previous section that the eigenfunctions associated with each of these operators is doubly degenerate. In fact the eigenfunctions depicted in Fig. 5 correspond to K_1^{-}. Alternately it is associated with the projector

$$E_1^{-} = Z^{-} E_1 = \frac{I-Z}{2}\frac{I-Q}{2} = \frac{1}{4}(I - Z - Q + ZQ) \tag{73}$$

in the sense that it is invariant under this transformation. It also follows from the discussion in Sec. V that rotation of the flow around the vertical in Fig. 5 by $\pi/2$ is the second eigenfunction of the invariant subspace.

In the actual calculation the flow is primarily made up of the two eigenfunctions (i.e., the invariant subspace of the principal eigenvalue) that correspond to the picture in Fig. 5 (more than 50% of the energy on the average lies in this invariant subspace). At random times this cell-like flow rotates by $\pi/2$. On average the flow spends equal time in these two most probable states. This motion is explored in more detail in (II).

A second eigenfunction is actually depicted in Fig. 3. Although it was referred to as the mean flow earlier, it was also mentioned that there is some fine print. To explain this further point we denote the mean flow in one particular simulation by $\bar{\mathbf{u}}$, then group-averaged mean flow is given by

$$\langle \bar{\mathbf{u}} \rangle = \frac{1}{16}\sum_{l=1}^{16} g_l \bar{\mathbf{u}} = Z^{+} E_5 \bar{\mathbf{u}} = E_5^{+} \bar{\mathbf{u}}.$$

It therefore follows that $\langle \bar{\mathbf{u}} \rangle$ can be represented in terms of the eigenfunction of $\mathbf{K}_5^{+}$. Figure 3 actually represents the principal eigenfunction of $\mathbf{K}_5^{+}$. The error in this approximation to the mean flow is only 2.4% in the energy norm.

ACKNOWLEDGMENTS

We express grateful thanks to Bruce Knight for introducing us to the mysteries of group representation methods. Computations were performed on the Cyber 205 Supercomputer at the John von Neumann National Computer Center.

This work reported here was supported by DARPA-URI N00014-86-K0754.

APPENDIX: SYMMETRY CONSIDERATIONS FOR OTHER FLOWS

There are just a few essential features needed in the group operations, as presented in Secs. IV and V. In particular, we need the group under which the flow under considerations remain invariant. It is then essential to determine the list of projectors of the group. In the following we present three examples, out of the many that one can imagine, to further illustrate the basic steps.

1. Bénard convection in a rectangular box with fixed walls

The flow geometry is invariant under the dihedral group D_{2h} $(D \neq W)$ with the group elements.

$$D_{2h}: E, R_0^2, R_y, R_0^2 R_y, R_z, R_z R_0^2, R_z R_y, R_z R_0^2 R_y. \tag{A1}$$

The corresponding projectors are as follows:

$$E_1 = \tfrac{1}{8}(E + R_0^2 + R_y + R_0^2 R_y + R_0^2 R_z + R_z + R_z R_0^2 R_y + R_z R_y), \tag{A2}$$

$$E_2 = \tfrac{1}{8}(E + R_0^2 - R_y - R_0^2 R_y + R_0^2 R_z + R_z - R_z R_0^2 R_y - R_z R_y), \tag{A3}$$

$$E_3 = \tfrac{1}{8}(E - R_0^2 + R_y - R_0^2 R_y + R_0^2 R_z - R_z + R_z R_0^2 R_y - R_z R_y), \tag{A4}$$

$$E_4 = \tfrac{1}{8}(E - R_0^2 - R_y + R_0^2 R_y + R_0^2 R_z - R_z - R_z R_0^2 R_y + R_z R_y), \tag{A5}$$

$$E_5 = \tfrac{1}{8}(E + R_0^2 + R_y + R_0^2 R_y - R_0^2 R_z - R_z - R_z R_0^2 R_y - R_z R_y), \tag{A6}$$

$$E_6 = \tfrac{1}{8}(E + R_0^2 - R_y - R_0^2 R_y - R_0^2 R_z - R_z + R_z R_0^2 R_y + R_z R_y), \tag{A7}$$

$$E_7 = \tfrac{1}{8}(E - R_0^2 + R_y - R_0^2 R_y - R_0^2 R_z + R_z - R_z R_0^2 R_y + R_z R_y), \tag{A8}$$

$$E_8 = \tfrac{1}{8}(E - R_0^2 - R_y + R_0^2 R_y - R_0^2 R_z + R_z + R_z R_0^2 R_y - R_z R_y). \tag{A9}$$

2. Poiseuille flow in a rectangular channel with fixed side walls

The direction of mean flow is denoted by x, the spanwise direction by y and the vertical by z. If $\mathbf{V}^{(n)}(\mathbf{x})$ is a flow realization or snapshot at some instant, then the fluctuating component of $\mathbf{V}^{(n)}(\mathbf{x})$ satisfies the following transformation:

$$T_x:\mathbf{V}^{(n)}\rightarrow\mathbf{V}^{(n)}(x+l_1,y,z). \tag{A10}$$

It therefore follows that averaging over the groups (A10) implies

$$\mathbf{K}(\mathbf{x},\mathbf{x}')=\mathbf{K}(x-x',y,z), \tag{A11}$$

i.e., the two-point correlation is translationally invariant or homogeneous in the mean flow direction and the correlation tensor in that direction is represented by sinusoids.

This flow geometry is also invariant under the dihedral group of transformations, D_2 with group elements,

$$D_2:E,R_0^2,R_y,R_z. \tag{A12}$$

The corresponding projectors are

$$E_1=\tfrac{1}{4}(E+R_0^2+R_y+R_z), \tag{A13}$$

$$E_2=\tfrac{1}{4}(E+R_0^2-R_y-R_z), \tag{A14}$$

$$E_3=\tfrac{1}{4}(E-R_0^2+R_y-R_z), \tag{A15}$$

$$E_4=\tfrac{1}{4}(E-R_0^2-R_y+R_z). \tag{A16}$$

If $L_y=L_z=L$, the problem is invariant under the dihedral group D_4.

$$D_4:E,R_0,R_0^2,R_0^3,R_y,R_0R_y,R_0^2R_y,R_0^3R_y \tag{A17}$$

and the corresponding projectors are presented in Sec. IV.

3. Taylor–Couette flow

The axis of rotation is taken in the x direction and cylindrical coordinates (x,r,θ). The invariance group is now composed of translation in the x direction, T_x; reflection in the plan normal to x, R_x, and rotation around the x axis, T_θ.

The relevant discrete group is

$$C_{1h}:E,R_x \tag{A18}$$

and the corresponding projectors are given by

$$E_1=\tfrac{1}{2}(E+R_x), \tag{A19}$$

$$E_2=\tfrac{1}{2}(E-R_x). \tag{A20}$$

It should be observed that for these deliberations as well as for those in Secs. IV and V, the question of slip or nonslip boundaries is not a factor.

[1] R. B. Ash and Gardner M. F. *Topics in Stochastic Processes* (Academic New York, 1975).
[2] J. L. Lumley, in *Transition and Turbulence*, edited by R. E. Meyer (Academic, New York, 1981), pp. 215–242.
[3] J. L. Lumley, *Stochastic Tools in Turbulence* (Academic, New York, 1970).
[4] J. L. Lumley, in *Atmospheric Turbulence and Radio Wave Propagation*, edited by A. M. Yaglom and V. I. Tatarski (Nauka, Moscow, 1967), pp. 166–178.
[5] L. Sirovich, Physica D **37**, 126 (1989).
[6] F. R. Payne and J. L. Lumley Phys. Fluids **10**, S 194 (1967).
[7] M. N. Glauser, S. J. Lieb, and N. K. George, in *Proceedings of the 5th Symposium on Turbulent Shear flow*, Cornell Univ. (Springer, New York, 1985), pp. 134–145.
[8] P. Moin and R. D. Moser, J. Fluid Mech. **200**, 471 (1988).
[9] H. Park and L. Sirovich, Phys. Fluids A **2**, 1659 (1990).
[10] P. Moin and J. Kim, J. Fluid Mech. **118**, 341 (1982).
[11] P. Moin and J. Kim, J. Fluid Mech. **155**, 441 (1985).
[12] J. H. Herring and J. Wyngaard, in Ref. 7, pp. 10.39–10.43.
[13] L. Sirovich, M. Maxey, and H. Tarman, Bull. Am. Phys. Soc. **30**, 1676 (1986).
[14] L. Sirovich, H. Tarman, and M. Maxey, in Sixth Symposium of Turbulent Shear Flow, Toulouse, France, 1987.
[15] L. Sirovich, H. Tarman, and M. Maxey, *An Eigenfunction Analysis of Turbulent Thermal Convection*, (Springer, New York, 1988), pp. 68–80.
[16] Lord Rayleigh, Philos. Mag. **32**, 529 (1916).
[17] A. Pellew and R. V. Southwell, Proc. R. Soc. London Ser. A **176**, 312 (1940).
[18] S. H. Davis, J. Fluid Mech. **30**, 465 (1967).
[19] G. Birkhoff, *Hydrodynamics: A Study in Logic, Fact and Similitude*, (Princeton U.P., Princeton, NJ, 1950).
[20] L. I. Sedov, *Similarity and Dimensional Methods in Mechanics* (Academic, New York, 1959).
[21] G. I. Barenblatt, *Similarity, Self Similarity, and Intermediate Asymptotics* (Consultants Bureau, New York, 1979).
[22] M. Golubitsky, I. Stewart, and D. G. Schaeffer, *Singularities and Groups in Bifurcation Theory* (Springer, New York, 1988), Vol. II.
[23] D. McKenzie, J. Fluid Mech. **191**, 287 (1988).
[24] P. G. Drazin and W. H. Reid, *Hydrodynamic Stability* (Cambridge U.P., London, 1981).
[25] S. Chandrasekhar, *Hydrodynamic and Hydromagnetic Stability* (Oxford U.P., London, 1961).
[26] L. Sirovich, Q. Appl. Math. **XLV**, (3), 561 (1987).
[27] J. P. Gollub, and S. V. Benson, J. Fluid Mech. **100**, 449 (1980).
[28] D. Malraison, P. Atten, P. Bergé, and M. Dubois, C. R. Acad. Sci. Paris, **C297**, 209 (1983).
[29] A. E. Deane and L. Sirovich, submitted to J. Fluid Mech.
[30] L. Sirovich and A. E. Deane, submitted to J. Fluid Mech.
[31] L. Sirovich and J. D. Rodriguez, Phys. Lett. A **120**, 211 (1987).
[32] S. G. Mikhlin, *Integral Equations* (MacMillan, New York, 1964).
[33] L. Sirovich and M. Kirby, J. Opt. Soc. Am. A **4**, 519 (1987).
[34] M. Kirby and L. Sirovich, submitted for publication.
[35] L. Sirovich, Q. Appl. Math. **XLV** (3), 573 (1987).
[36] M. Hall, *The Theory of Groups* (MacMillan, New York, 1965).
[37] M. Burrow, *Representation Theory of Finite Groups* (Academic, New York, 1965).
[38] G. I. Taylor and A. E. Green, Proc. R. Soc. London Ser. A **158**, 499 (1937).
[39] S. A. Orszag, in *Fluid Dynamics, les Houches Summer School*, edited by R. Balian and J. L. Penbe (Gordon and Breach, New York, 1977).
[40] R. H. Morf, S. A. Orszag, and U. Frisch, Phys. Rev. Lett. **44**, 572 (1980).